# Boosting $CO_2$-to-$C_2H_4$ Electrocatalysis on $Cu_2O$ with Waste-Derived Porous Carbon from Coconut Shells

Chen Qin,[a†] TangRui Li,[a†] Gevindu Masakorala,[b†] ChengJie Zhi,[c] HongXiang Huang,[c,d], Chen Zhou,[a] Xue Wang,[e] Bo Shen,[f] Jian-Rong Zhang,[a] Yang Zhou,[c,*] Charitha Thambiliyagodage[b,*], Wenlei Zhu,[a,*]

[a] State Key Laboratory of Water Pollution Control and Green Resource Recycling, State Key Laboratory of Analytical Chemistry for Life Science, Frontiers Science Center for Critical Earth Material Cycling, School of the Environment, School of Chemistry and Chemical Engineering, Nanjing University, Nanjing 210023, China

[b] Department of Applied Sciences, Faculty of Humanities and Sciences, Sri Lanka Institute of Information Technology, Malabe 10115, Sri Lanka

[c] State Key Laboratory of Flexible Electronics & Institute of Advanced Materials (IAM), Nanjing University of Posts & Telecommunications, Nanjing 210023, China

[d] School of Pharmacy, China Pharmaceutical University, Nanjing 210009, China

[e] School of Energy and Environment, State Key Laboratory of Marine Environmental Health, City University of Hong Kong, Hong Kong, 999077, China.

[f] Department of Materials Science and Engineering, City University of Hong Kong, Hong Kong, 999077, China.

[+] These authors contributed equally to this work.

* Corresponding authors emails: wenleizhu@nju.edu.cn; iamyangzhou@njupt.edu.cn; charitha.t@sliit.lk

## Catalysts Preparation

### Materials

Coconut husk was collected from the Kuliyapitiya area, Sri Lanka. Copper (II) sulfate pentahydrate ($CuSO_4 \cdot 5H_2O$, AR), hydrazine hydrate aqueous solution ($N_2H_4 \cdot H_2O$, 85.0% of volume fraction), Potassium bicarbonate ($KHCO_3$, AR) were purchased from Sinopharm Chemical Reagent Co., Ltd (Shanghai, China). Polyvinyl pyrrolidone (PVP, MW=55000, AR) and Nafion (5 wt%) were purchased from Macklin. Dimethyl sulfoxide and deuterium water were purchased from Rhawn. All chemicals were used as received without further purification.

### Synthesis catalysts

**Synthesis of Porous Coconut husk (PC) and Activated Coconut husk (AC).** The raw porous material coconut husk (CH) used is harvested in Sri Lanka. The soil and dust in the CH were washed with distilled water and ethanol and dried at 80℃. Then the CH were separately treated with 2 mol $dm^{-3}$ HCl at 60℃ for 2 h with regular stirring. Acid-leached CH was rinsed with distilled water until the pH of the filtrate reached ~ 6 and was dried at 80℃. Then the CH were placed in a muffle furnace and heated at 400℃ for 2h to obtain PC. All the prepared PC were activated with 6 M $HNO_3$ acid at 60℃ for 6 h with regular stirring. After the treatment, adsorbents were rinsed with distilled water until the pH of the washings reached ~ 6 and were dried at 80℃. The dried samples were sifted through sieves of 0.5 mm pore size to obtain the AC ,which was stored in a desiccator until further use.

**Synthesis of $Cu_2O$.** 300 mg of PVP was added into 30 mL of 0.01 M $CuSO_4$ aqueous solution under magnetic stirring (300 rpm). The mixture was kept stirring for several minutes until the powders were completely dissolved. $N_2H_4 \cdot H_2O$ solution (10 μL) was then introduced into the mixture solution, forming the orange colloidal suspension of $Cu_2O$ particles immediately. Thereafter, the resulting colloidal solution was further stirred (300 rpm) for 0.5 h for Ostwald ripening, resulting in the formation of the $Cu_2O$ single-layer nanoshells. Finally,

the nanoshells were centrifuged, washed with deionized water and ethanol, and dried overnight in a vacuum oven at 60°C to yield $Cu_2O$.

**Synthesis of $Cu_2O$-5mgC, $Cu_2O$-10mgC, $Cu_2O$-20mgC catalysts.** Take 5 mg, 10 mg, and 20 mg of AC respectively and dissolve each in 10 ml of water, followed by ultrasonic treatment for 30 minutes. Then, add 20 mg of $Cu_2O$ powder into three sample vials, and ultrasonicate for 30 minutes to allow $Cu_2O$ to load onto the AC. Subsequently, wash the samples multiple times with deionized water and ethanol, centrifuge, and dry them in vacuum oven (60℃ 12h) to collect the final products.

**Catalysts Characterization**

Scanning electron microscope (SEM) images were obtained on a JSM-7800F (JEOL, Japan). X-ray diffraction (XRD) data were recorded using a Shimadzu XRD-6000 diffractometer, with Cu Kα radiation (SHIMADZU, Japan). Transmission electron microscopy (TEM) characterization was conducted using a JEM-2800 electron microscope (JEOL, Japan) operated at 200 kV. X-ray photoelectron spectroscopy (XPS) was performed using a PHI 5000 VersaProbe (Ulvac-Phi, Japan) with an Al Kα (1486.6 eV) excitation source. *In-situ* Raman spectra were collected on a Horiba LabRAM HR Evolution spectroscopy at the excitation wavelength of 633 nm using a catalyst-coated gas diffusion layer as the working electrode. FTIR spectra were obtained using a Thermo Scientific NICOLET iS50.

**Electrochemical Measurements**

All electrochemical measurements were conducted on an electrochemical workstation (Gamry Interface 1000E). To prepare the cathode electrode, a mixture that contains 5 mg of catalysts, 2 mL of isopropanol, and 50 μL of Nafion ionomer solution (5 wt% in isopropanol) was first sonicated for 60 min to obtain a catalyst ink. Then, 2 mL of the catalyst ink was sprayed onto a gas diffusion layer to achieve a catalyst loading of ~0.8 mg $cm^{-2}$. Electrochemical tests were

conducted in an electrochemical flow cell, which includes a gas chamber, a cathodic chamber, and an anodic chamber. A 0.5 M $KHCO_3$ solution was used as the anolyte and catholyte. A proton exchange membrane (Nafion N115) was used to separate the anodic and cathodic chambers. A piece of titanium mesh loaded with Iridium dioxide was used as the counter electrode, and a saturated Ag/AgCl was used as the reference electrode. The high-purity $CO_2$ (99.999%, 20 cc) was introduced on the back side of the gas diffusion layer, and the electrolyte flowed in both cathodic and anodic chambers with a flow rate of 2 mL $min^{-1}$. The electrochemically active surface area (ECSA) was determined by measuring double-layer capacitance ($C_{dl}$). $C_{dl}$ was determined by measuring the capacitive current associated with double-layer charging from the scan-rate dependence of the cyclic voltammogram (CV). All potentials were converted to the reversible hydrogen electrode by E (RHE) = E (Ag/AgCl) + 0.197 V + 0.0591 V × pH without iR compensation.

**Product Analysis**

The gaseous products were monitored by an online gas chromatograph (GC, GC9790PLUS) equipped with a thermal conductivity detector (TCD) and a flame ionization detector (FID). The liquid products in cathode chambers were collected after electrolysis and analyzed by $^1H$ nuclear magnetic resonance (NMR, Bruker AV400) using DMSO as the internal standard and $D_2O$ as a proton signal source.

The Faraday efficiency (FE) of gas products was calculated by the following equation:

$$FE\% = \frac{I}{I_{total}} = \frac{zFnV}{I_{total}} \times 100\%$$

Where I is the partial current density of a specific product. I total is the total current density collected in the bulk electrolysis at an applied potential. z is the number of electrons involved in the formation of a specific product. F is the Faraday constant, 96485 C $mol^{-1}$. n is the mole fraction of the product. V is the gas volumetric flow rate of gas.

The FE of the liquid products was calculated as:

$$FE = z \cdot F \cdot \frac{n}{Q}$$

Where z is the number of electrons transferred per mole of gas product, F is the Faraday constant (96500 C $mol^{-1}$), n is the total amount of the liquid products determined from NMR (mole), and Q is the total amount of charge passed through the cathode (A·s).

### *In-Situ* Raman Characterization

*In-situ* Raman measurements were conducted in a commercial spectro-electrochemical cell with a three-electrode configuration. To prepare the customized working electrodes, the obtained catalyst inks (5 mg/mL of each of the two catalysts: AC, Sn-5%) was uniformly dropped onto the carbon paper (39BB, purchased from Fuel Cell Store) with a 2 × 2 $cm^2$ area (catalyst loading ~1.0 mg/$cm^2$) and dried overnight at 60°C in a vacuum oven. The obtained carbon paper was then used as working electrodes, with a nickel tape and a saturated Ag/AgCl (filled with 3 M KCl) electrode as the counter electrode and reference electrode, respectively. *In-situ* Raman experiments were conducted on a confocal Raman spectrometer (Renishaw inVia-Reflex) with a laser wavelength of 633 nm. The spectrochemical cell was coupled to a CHI 660E electrochemical analyzer for the electrochemical measurements. Before *in-situ* experiments, background spectra were collected without any applied potential. Subsequently, *in-situ* spectra were recorded at stepped potentials from −0.9 to −1.5 V vs. RHE in 0.5 M $KHCO_3$. All spectra were recorded with a 4 $cm^{-1}$ resolution and 10 scans.

### *In-situ* FT-iR Characterization

FTIR measurements were conducted using a Thermo Scientific NICOLET iS50 equipped with a liquid nitrogen-cooled MCT detector. The experiment utilized a custom-designed in situ thin-layer FTIR cell, with a glassy carbon electrode loaded with the catalyst as the working electrode, a platinum sheet as the counter electrode, and an Ag/AgCl electrode as the reference electrode. Prior to the experiment, gas was bubbled into the electrolyte for 30 minutes until saturation.

### DFT calculation

All spin-polarized computational simulations were performed using density functional

theory as implemented in the Vienna ab initio simulation package (VASP).[1,2] The ion-electron interactions were treated with the projected augmented wave (PAW) pseudopotentials,[3] and the plane-wave basis set was cut off at 450 eV. Generalized gradient approximation with the revised Perdew-Burke-Ernzerhof (GGA-PBE) functional was used to determine the exchange correlation energy.[4,5] The Brillouin zone was sampled by the Monkhorst-Pack method with a 4×4×2 kpoint grid.[6] The energy and force convergence criteria were set to be $10^{-6}$ eV and 0.02 eV $Å^{-1}$, respectively.[7]

A Cu(111) model was constructed, and then -OH and COOH modifications were carried out on the model surface to simulate Cu-edges with hydroxyl and carboxyl groups. All models adopted a 4×4 supercell, containing five atomic layers. A 20Å vacuum region was inserted in the z direction to avoid surface interactions and dipole moments. During the optimization process, the bottom two layers were fixed, while the top three layers and the adsorbate were allowed to relax.

According to the method developed by Rossmeisl and Nørskov, the Gibbs free energy change (ΔG) of each reaction step was defined as,

$$\Delta G = \Delta E + \Delta E_{ZPE} - T\Delta S$$

where ΔE is the total energy difference between the reactant and product species adsorbed on catalyst surface obtained directly from DFT calculations, $\Delta E_{ZPE}$ is the change in zero-point energies, T is the temperature (298.15 K), and ΔS is the difference vibrational entropy. The zero-point energy and entropy corrections of the intermediate adsorbed species were obtained from the harmonic vibrational frequency calculations.

The adsorption energy of CO on models was defined as:

$$E_{ads}=E_{slab+CO} - E_{slab} - E_{CO}$$

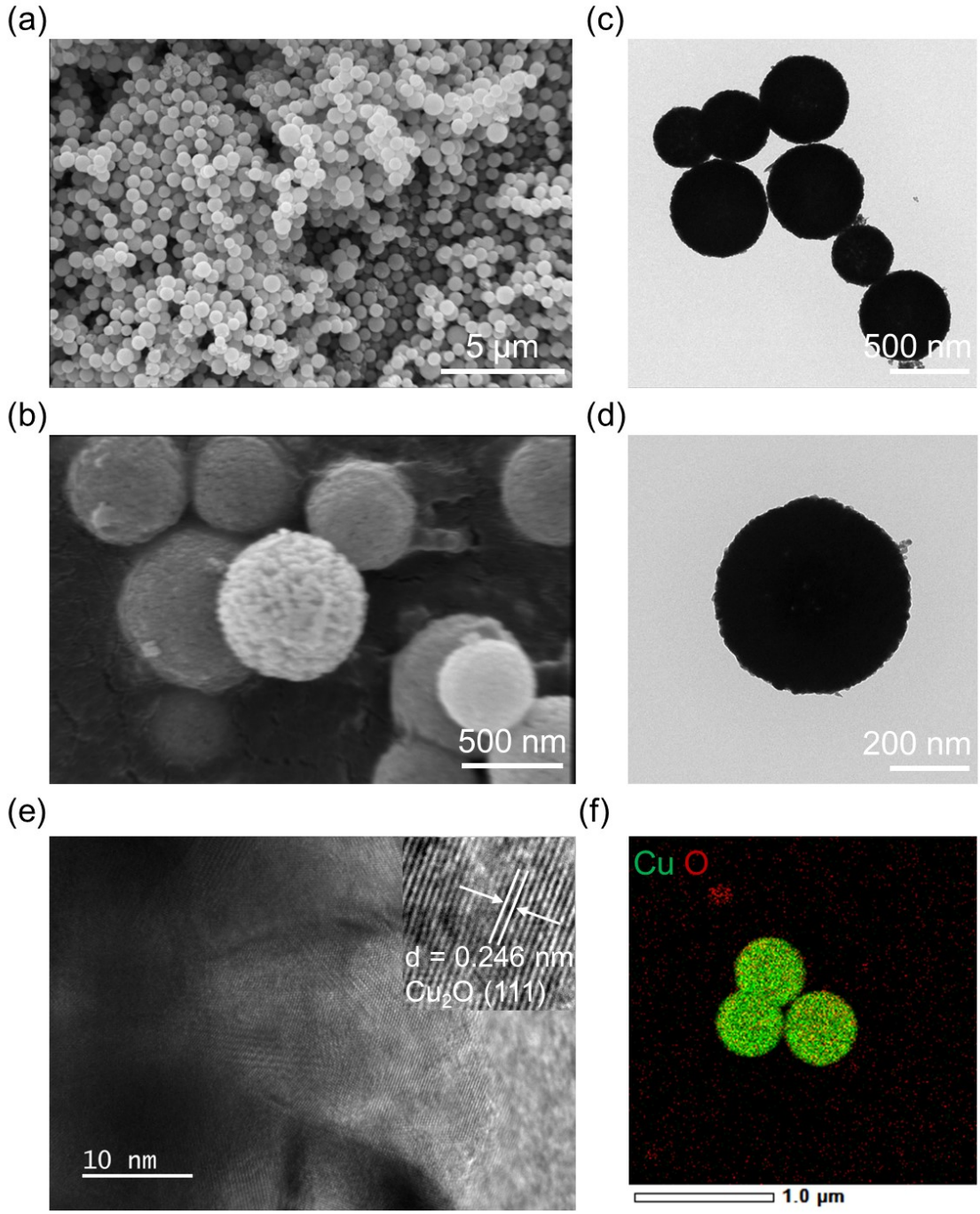


**Figure S1.** Morphological characterization of the $Cu_2O$ catalyst: (a) and (b) SEM images; (c) and (d) TEM images. (e) HRTEM image; (f) EDS mapping image.

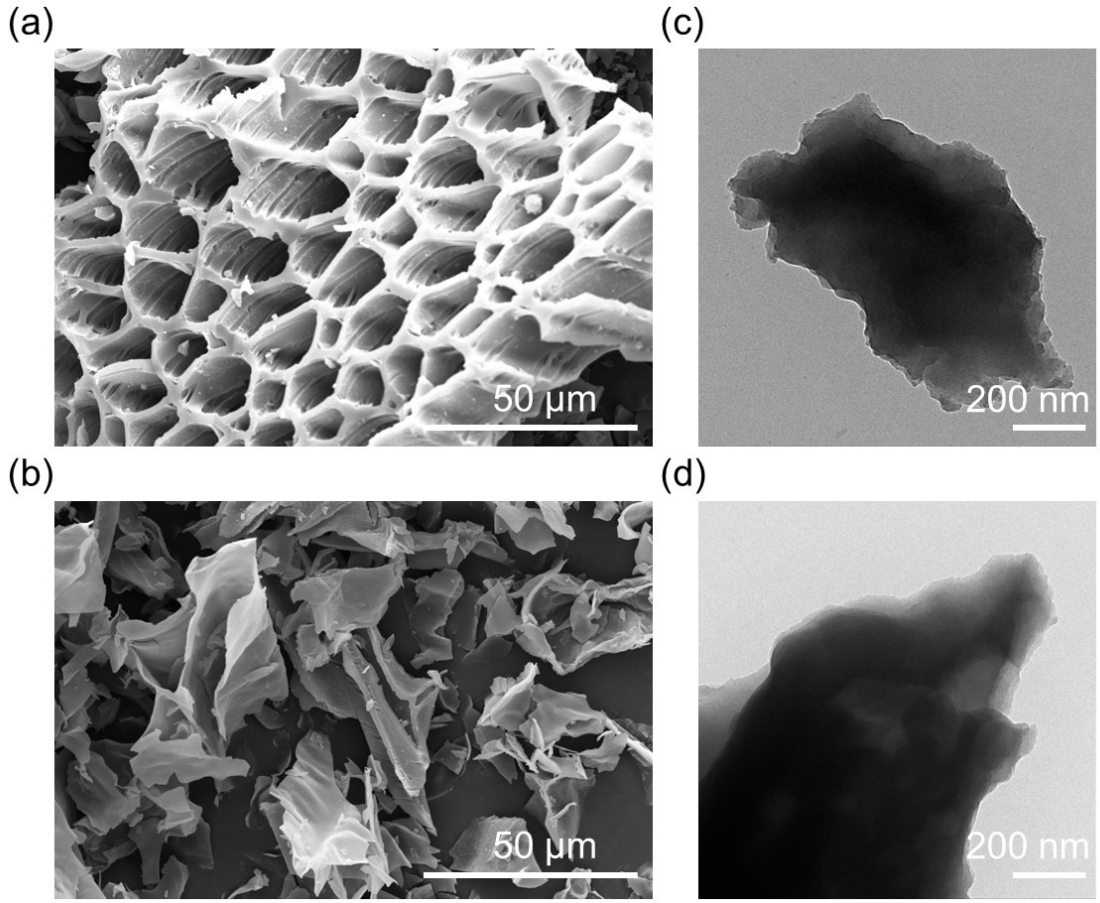


**Figure S2.** Morphological characterization of the PC catalyst: (a) and (b) SEM images; (c) and (d) TEM images.

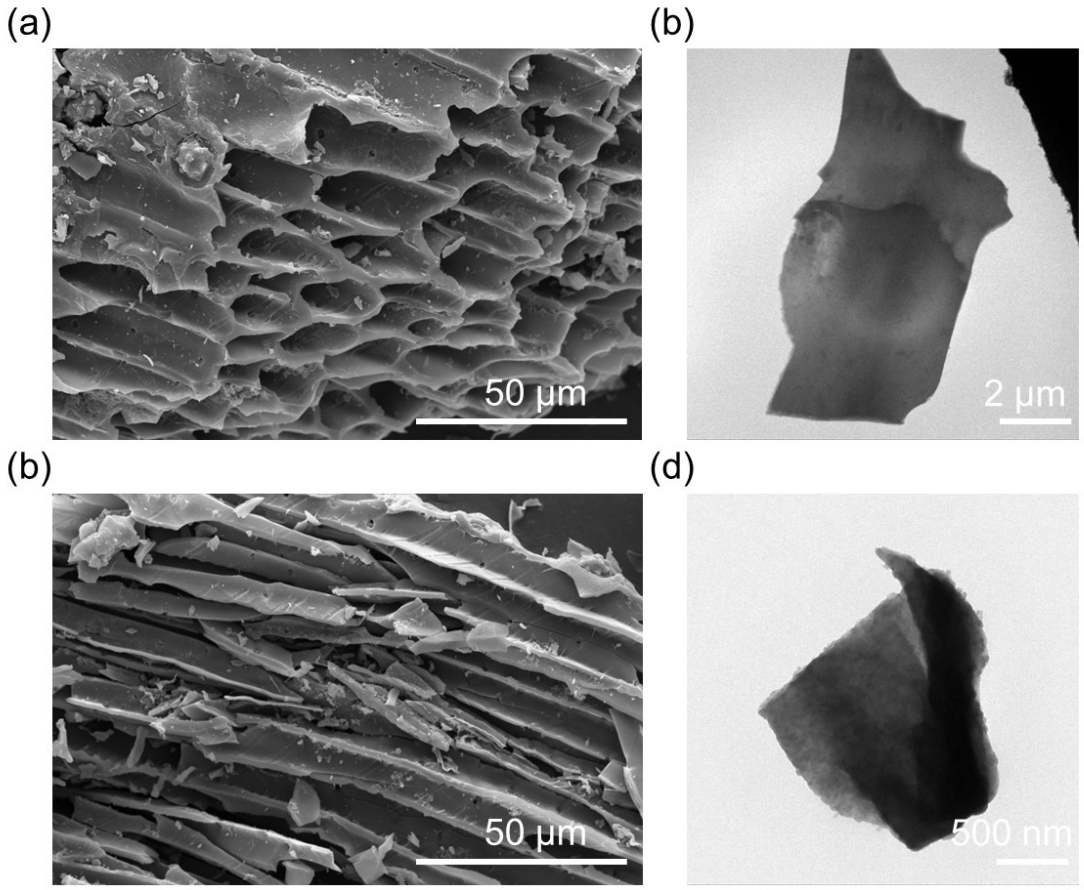


**Figure S3.** Morphological characterization of the AC catalyst: (a) SEM image; (b) TEM image.

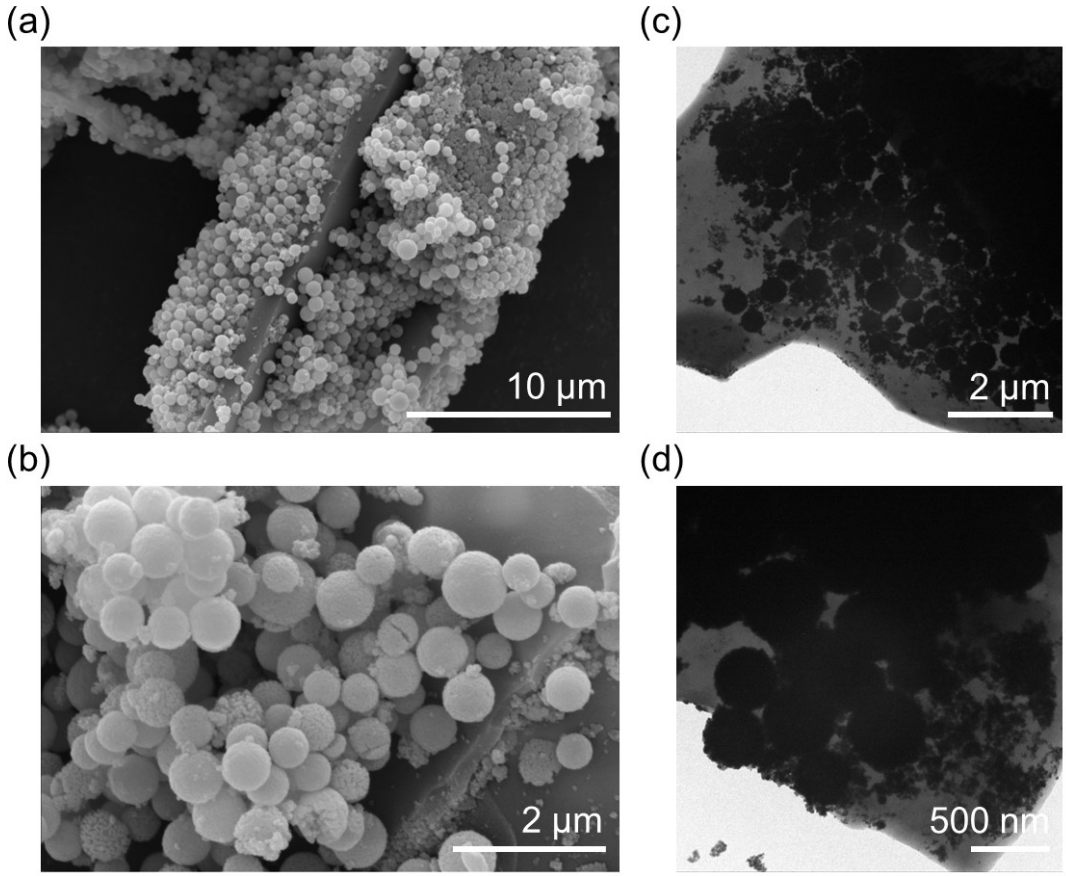


**Figure S4.** Morphological characterization of the $Cu_2O$-5mgC catalyst: (a) and (b) SEM images; (c) and (d) TEM images.

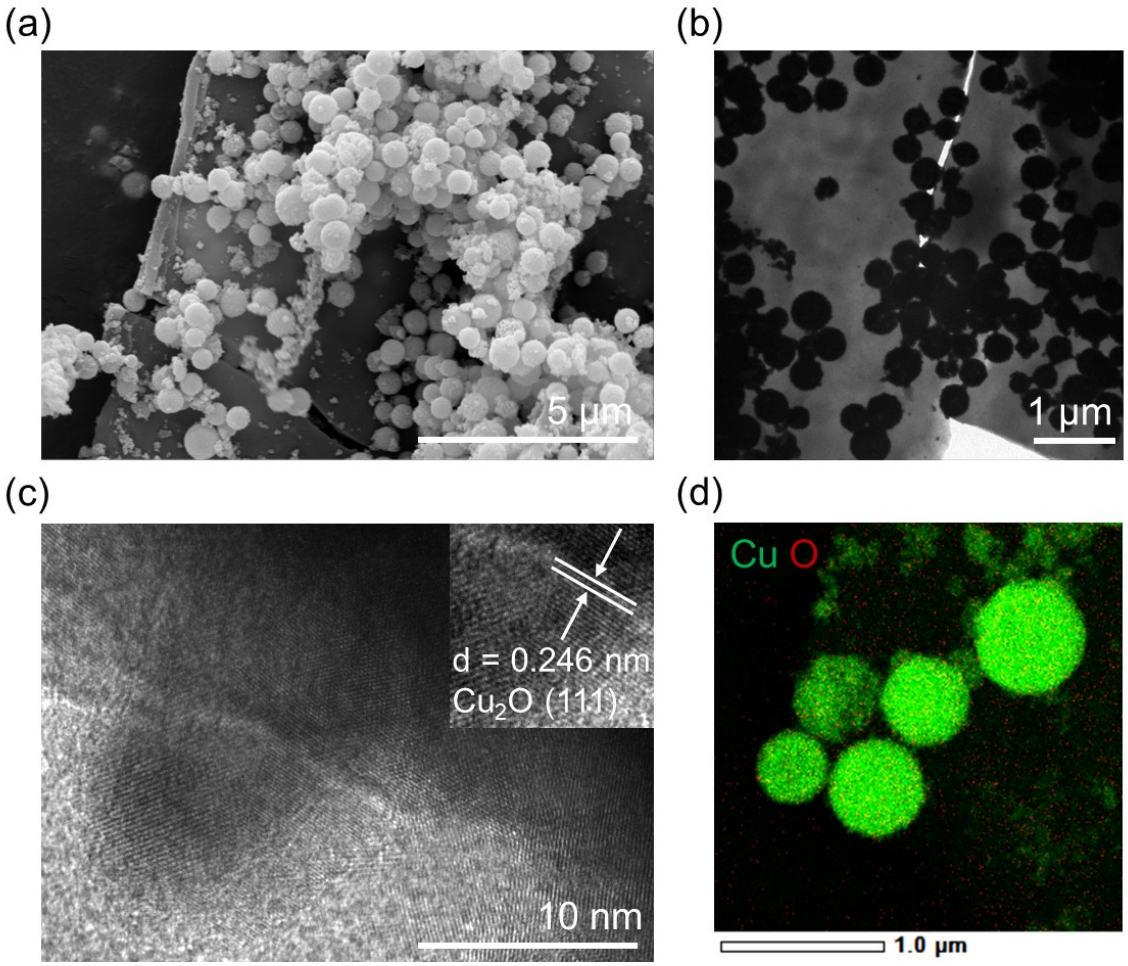


**Figure S5.** Morphological characterization of the $Cu_2O$-10mgC catalyst: (a) SEM image; (b) TEM image; (c) HRTEM image; (d) EDS mapping image.

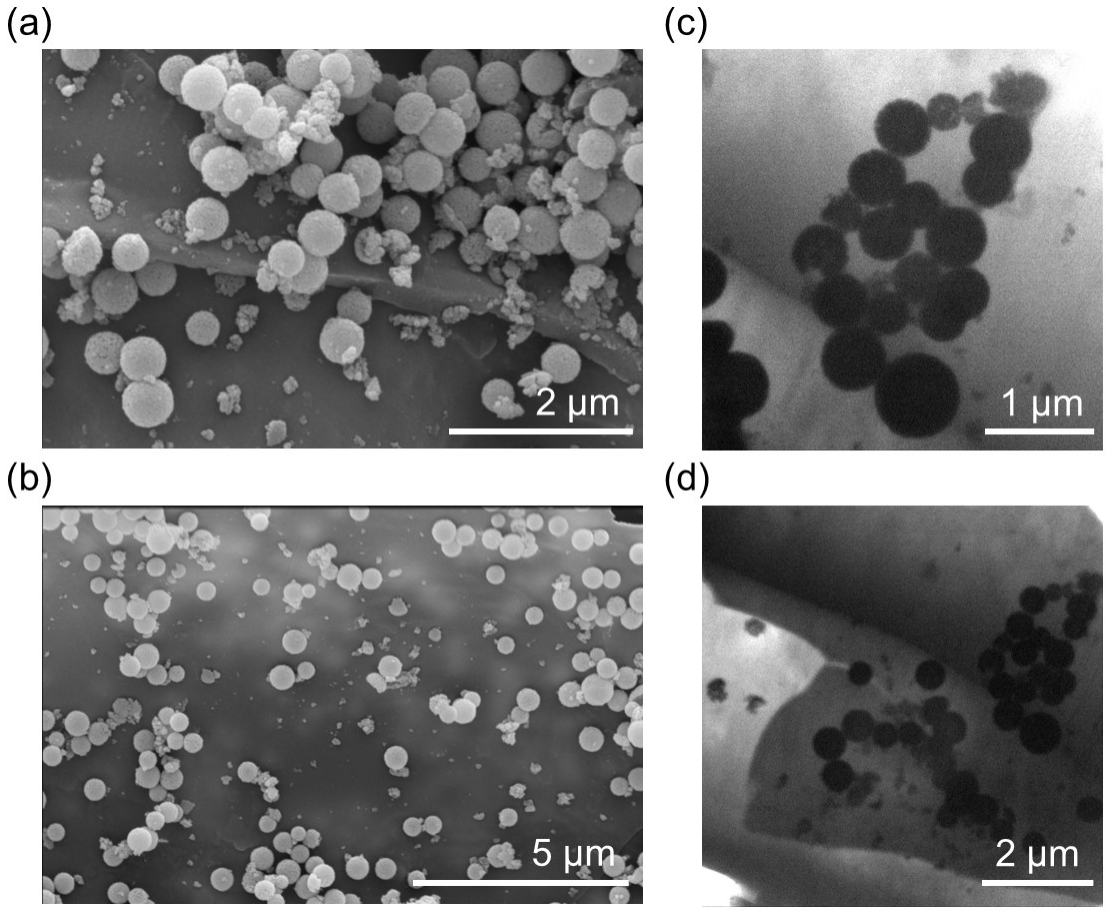


**Figure S6.** Morphological characterization of the $Cu_2O$-20mgC catalyst: (a) and (b) SEM images; (c) and (d) TEM images.

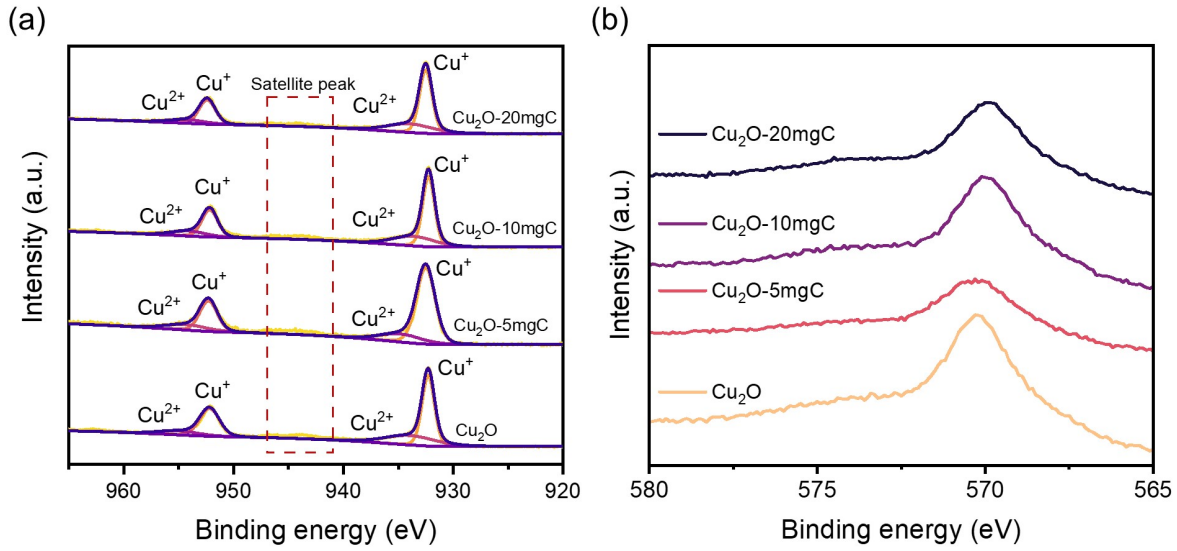


**Figure S7.** Higher resolution XPS spectra of (a) Cu 2p and (b) Cu LMM of different catalysts.

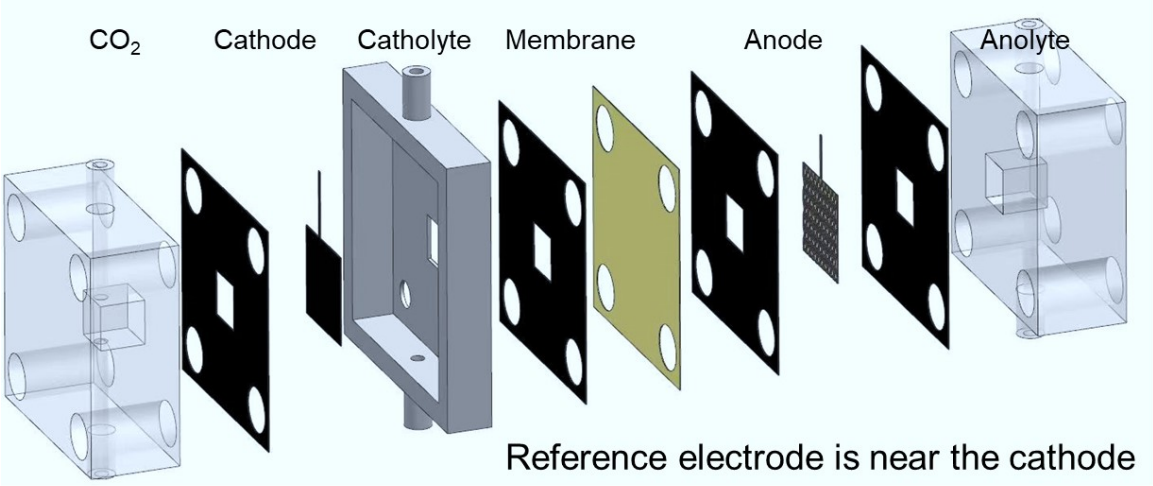


**Figure S8.** Schematic illustration of the flow-cell configuration.

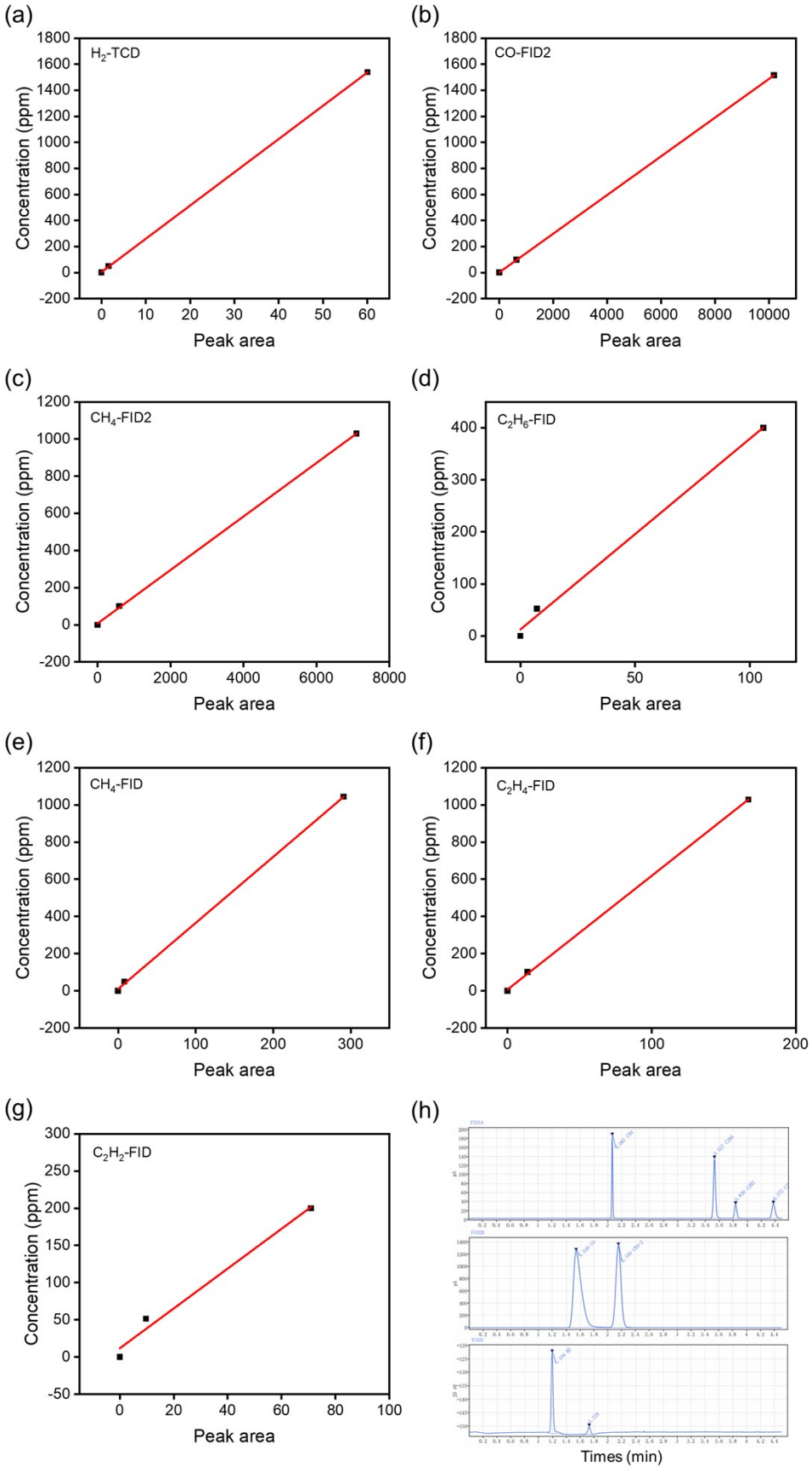


**Figure S9.** The calibration curves (a-g) and standardized GC chromatogram curves (h).

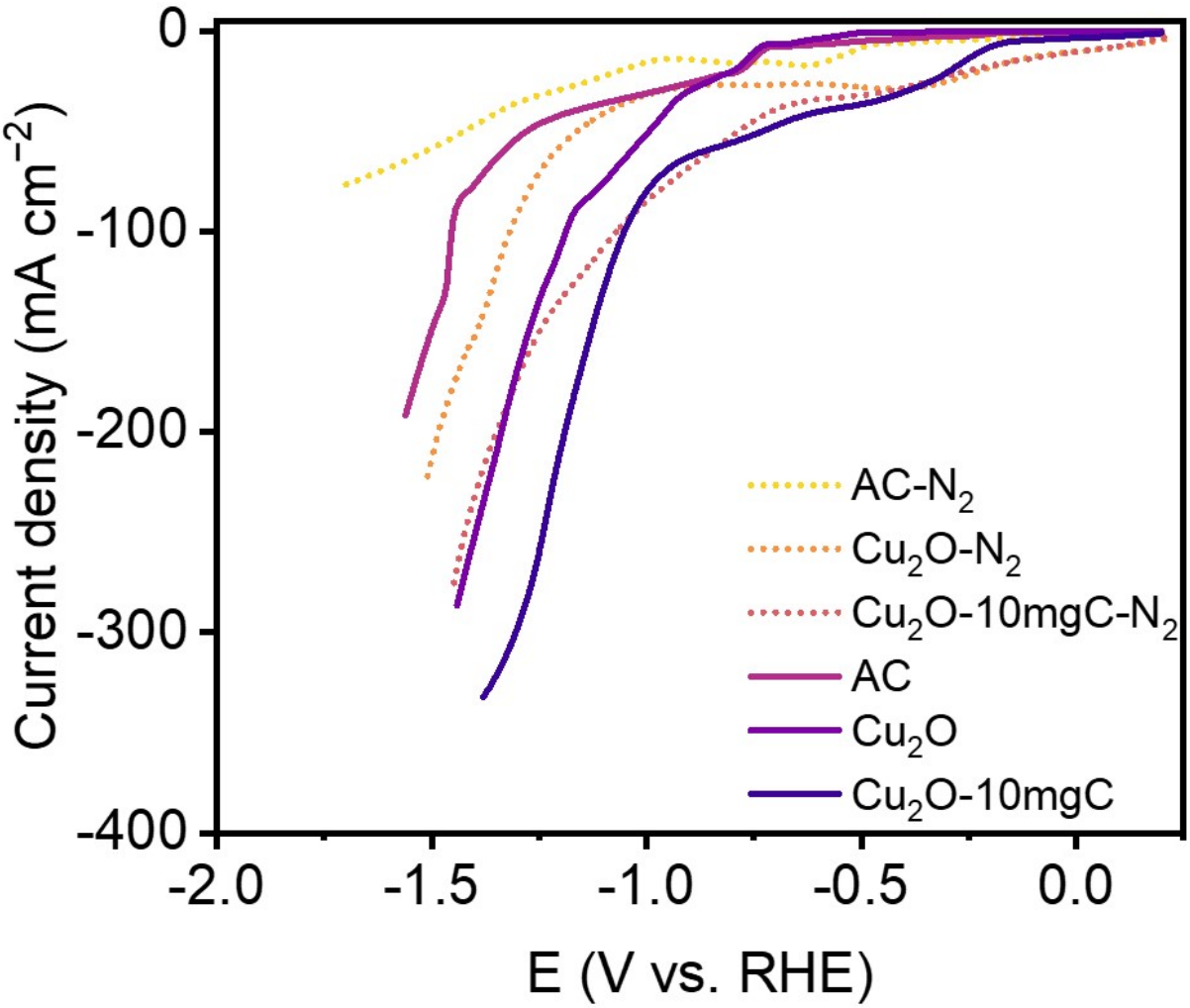


**Figure S10.** The linear sweep voltammetry curves in $N_2$-saturated and $CO_2$-saturated electrolytes.

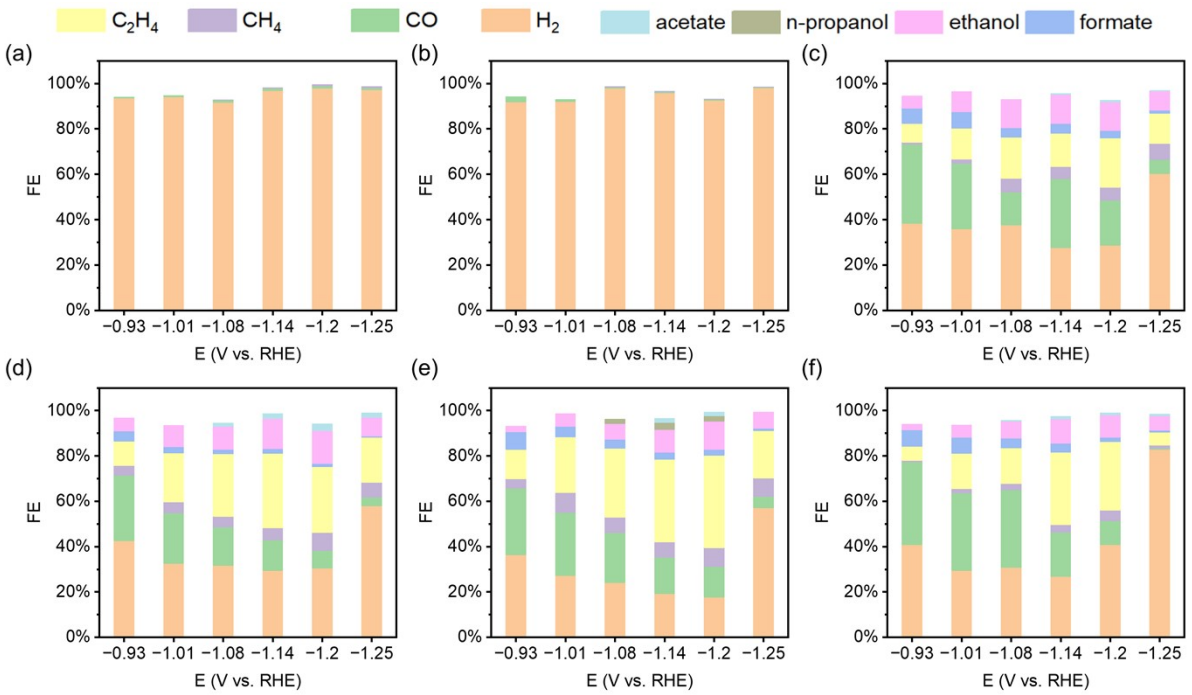


**Figure S11.** FEs of $CO_2$RR products on the catalyst in (a) PC, (b) AC, (c) $Cu_2O$, (d) $Cu_2O$-5mgC, (e) $Cu_2O$-10mgC, (f) $Cu_2O$-20mgC.

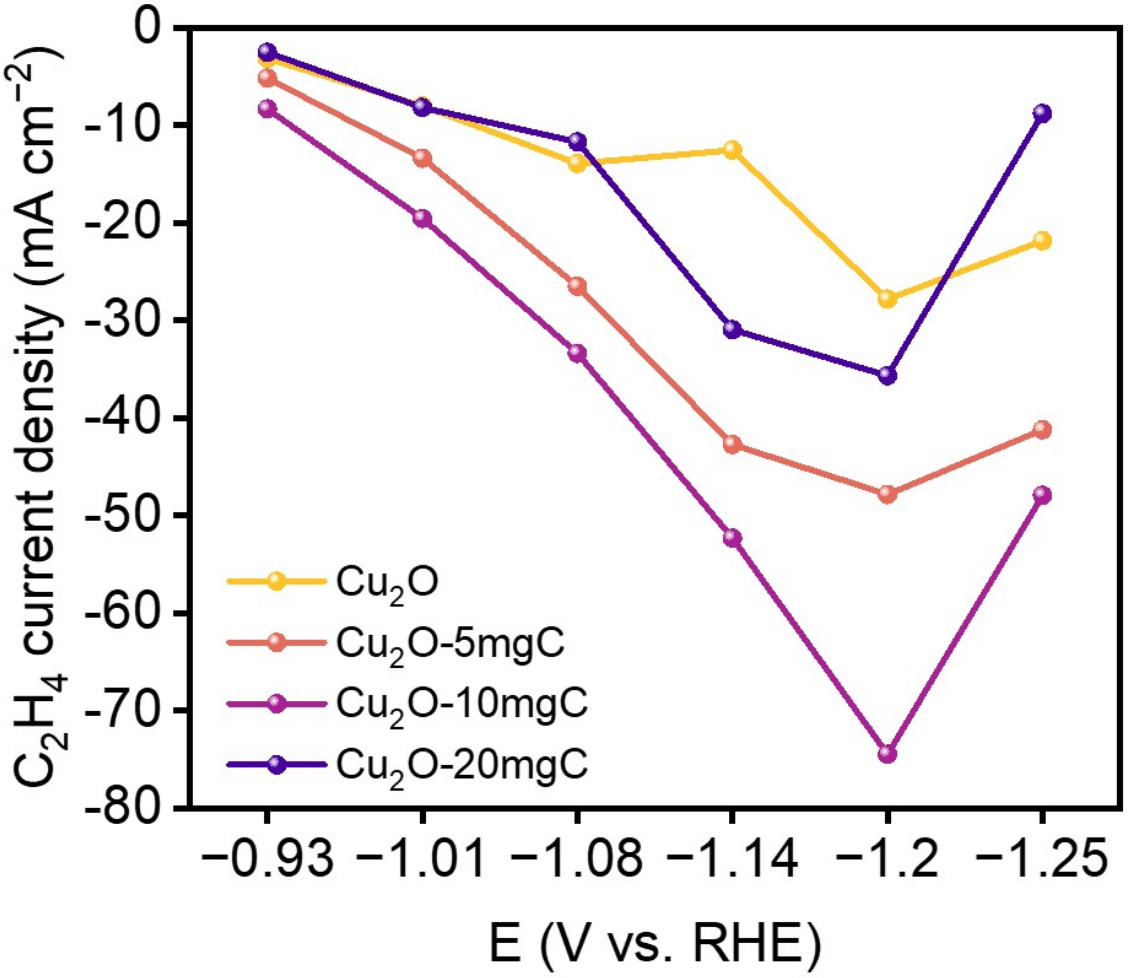


**Figure S12.** The $C_2H_4$ partial current densities on the different catalysts in different potentials.

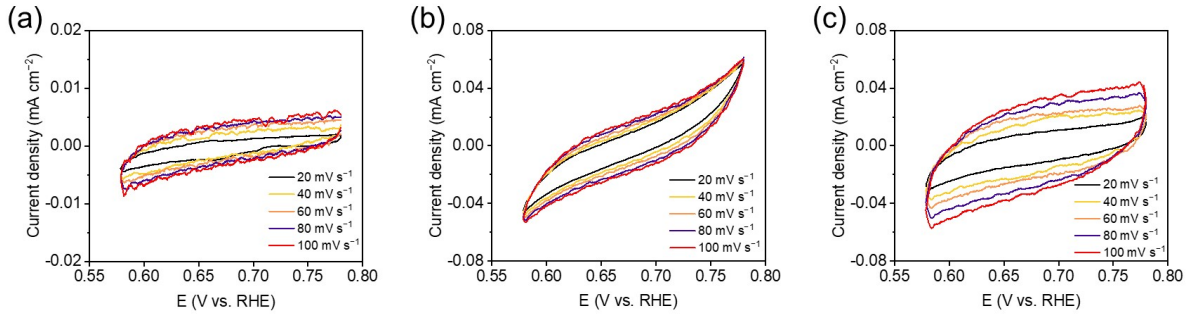


**Figure S13.** Cyclic voltammogram curves of different catalysts: (a) AC, (b) $Cu_2O$, (c) $Cu_2O$-10mgC at various scan rates (20, 40, 60, 80, and 100 mV $s^{-1}$).

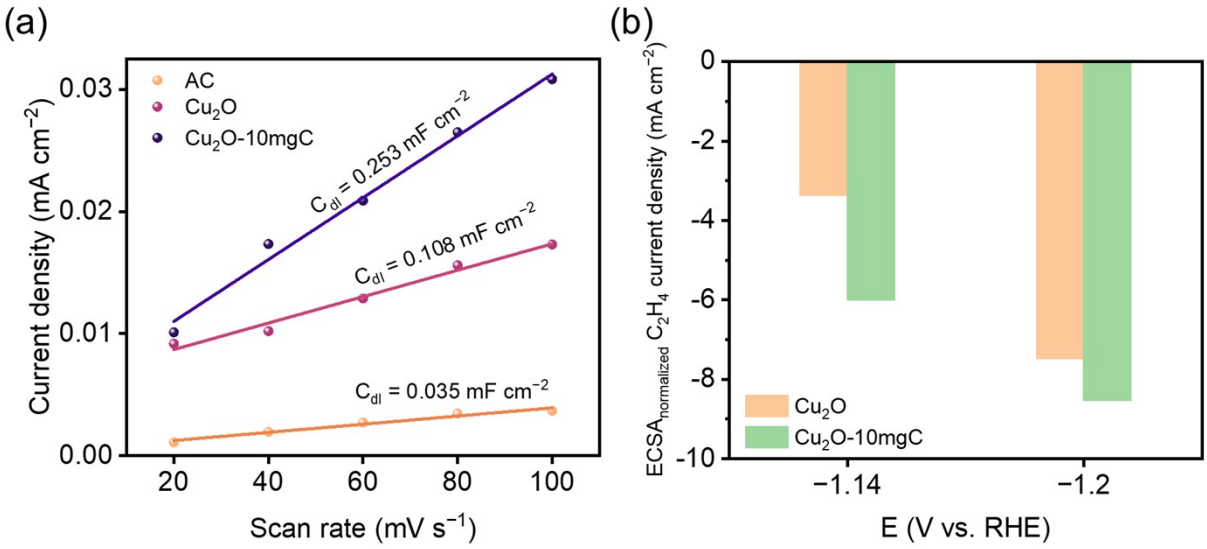


**Figure S14**. (a) Capacitive currents against scan rates at 0.95 V to obtain the double-layer capacities ($C_{dl}$, mF cm$^{-2}$ (electrode)) based on the slopes of these plots for Figure S11. (b) The ECSA normalized $C_2H_4$ partial current density in different potentials.

Electrochemically active surface area (ECSA, cm$^2$) was estimated as:

$$ECSA = C_{dl}$$

where $C_{gc}$ is the double layer capacitance (mF cm$^{-2}$) of the glassy carbon electrode surface, for which the typical value of 0.029 mF cm$^{-2}$ was used.

ECSA normalized $C_2H_4$ partial current density was calculated by $C_2H_4$ partial current density/ECSA.

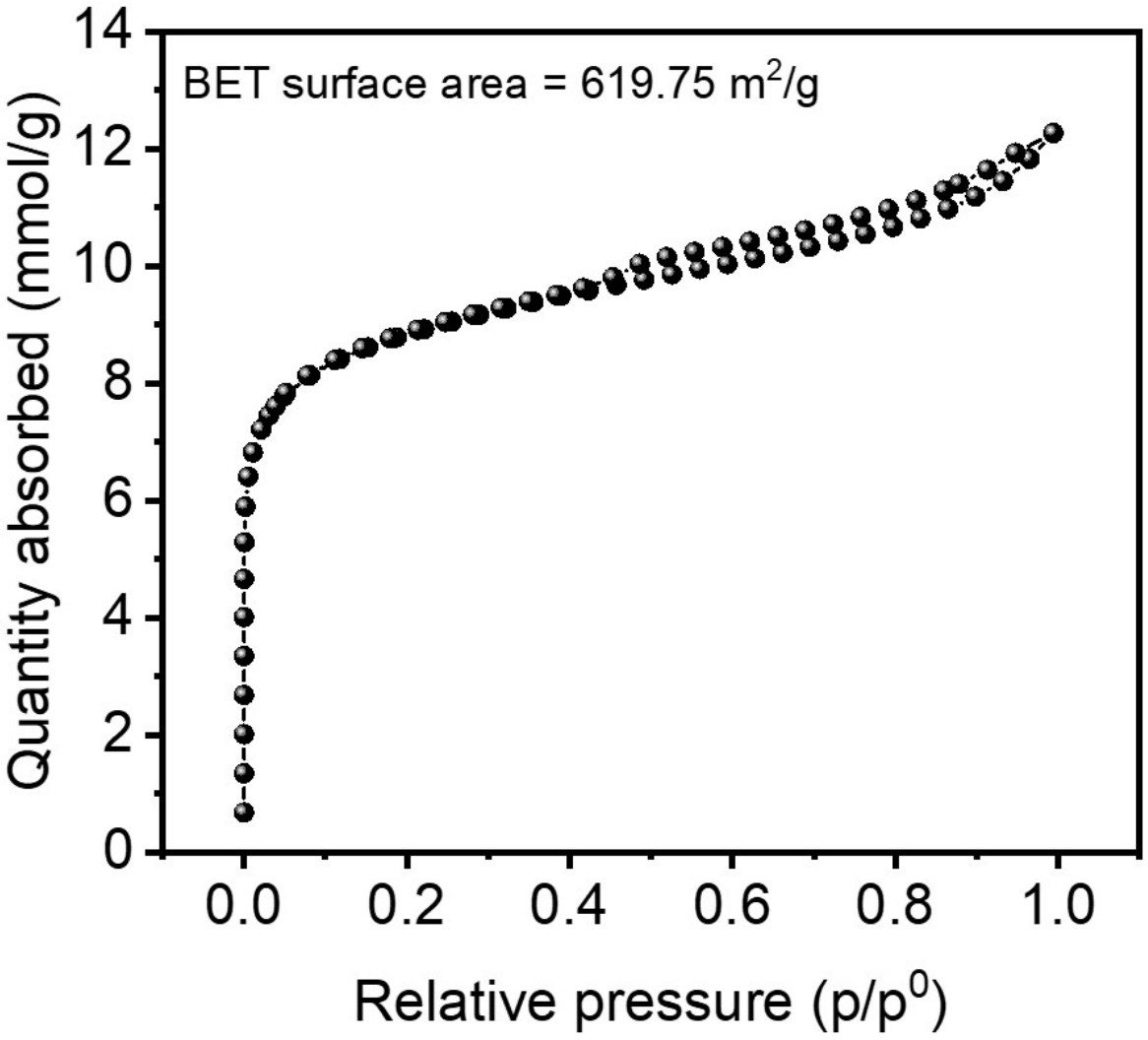


**Figure S15.** 77 K $N_2$ adsorption-desorption isotherms of AC.

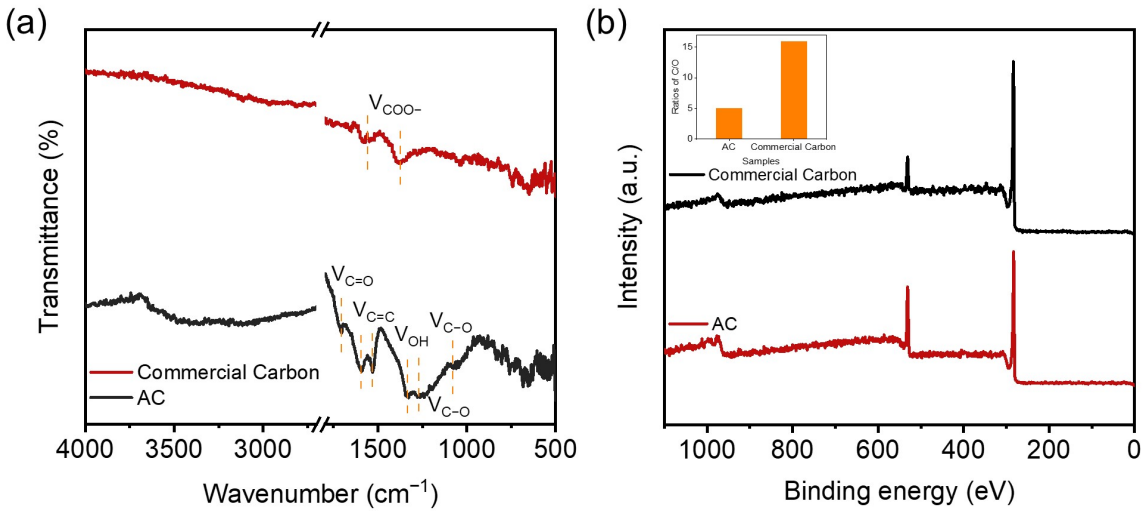


**Figure S16**. (a) FT-iR.spectra and (b) XPS all spectrum of AC and Commercial Carbon.

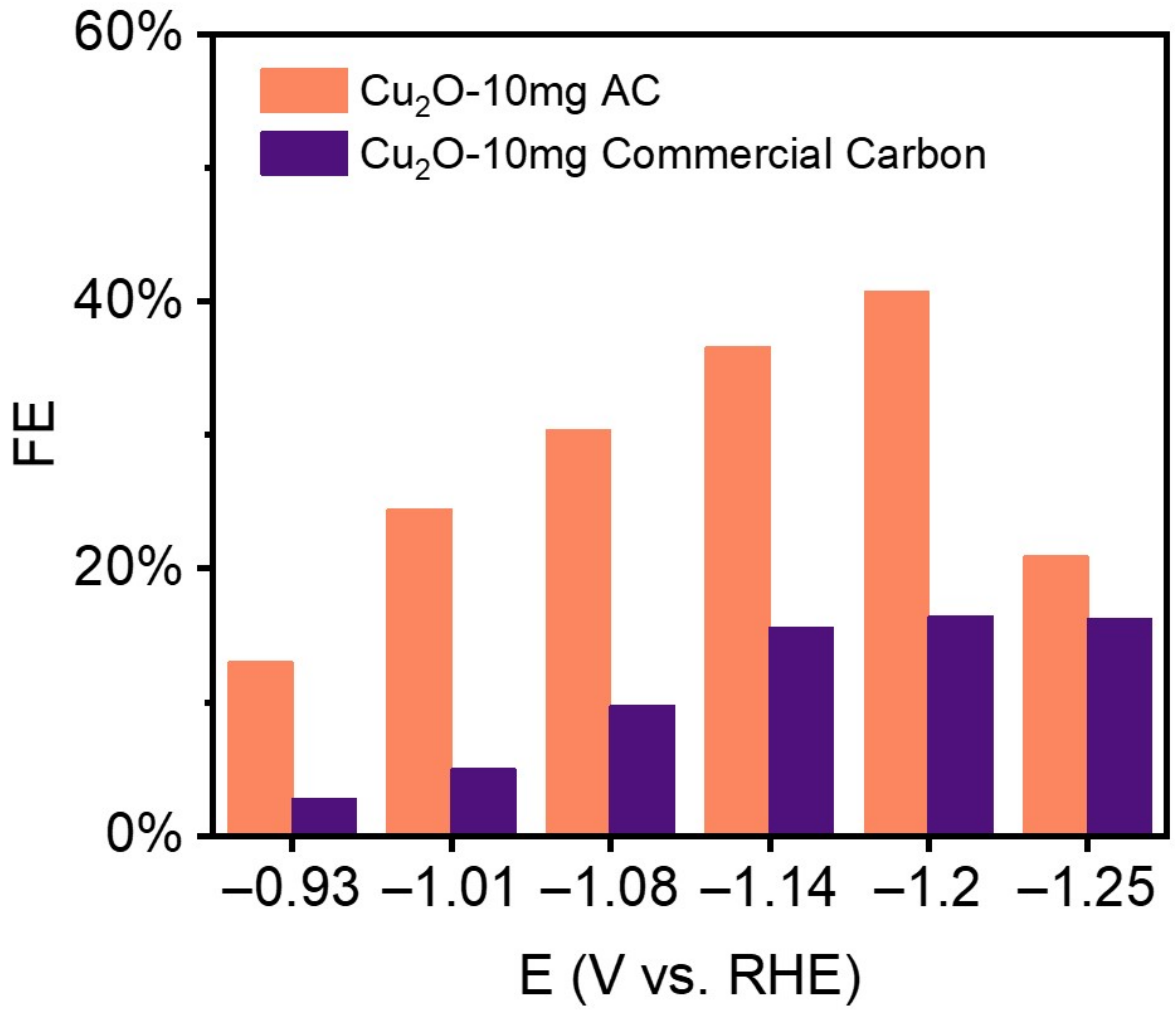


**Figure S17**. FE $C_2H_4$ of: (a) $Cu_2O$ in AC; (b) $Cu_2O$ in Commercial Carbon.

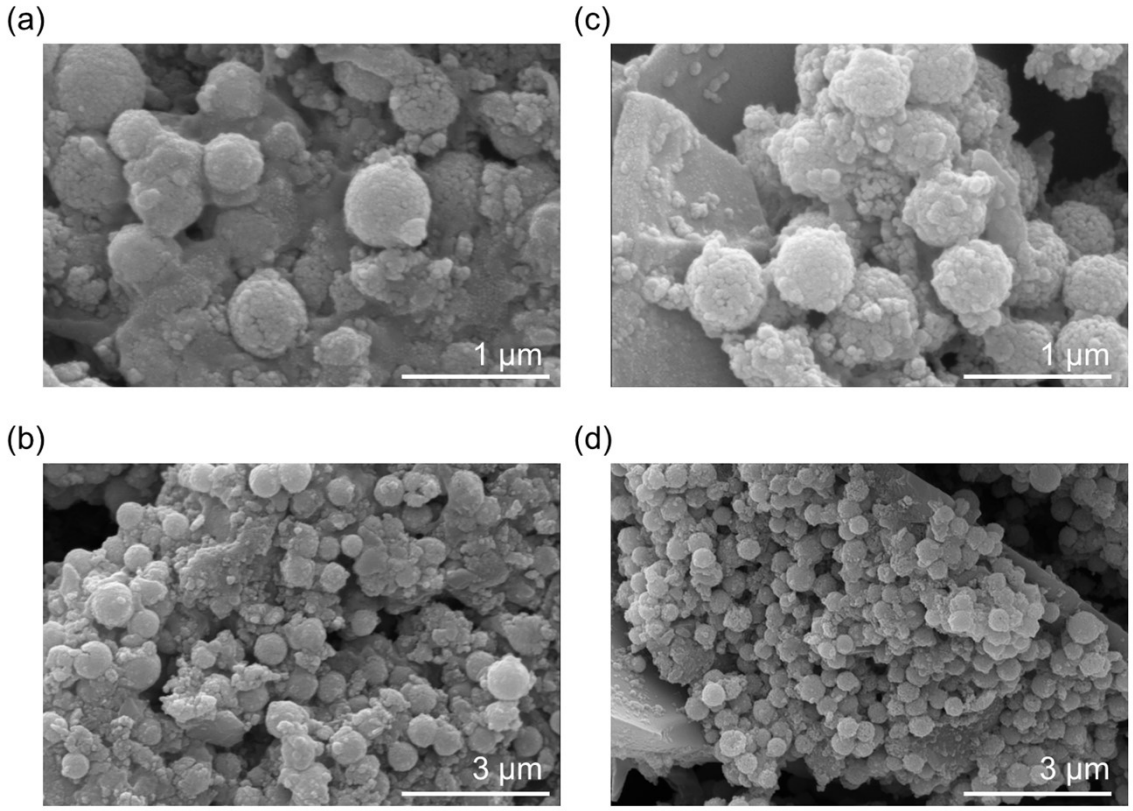


**Figure S18**. SEM images of (a-b) $Cu_2O$; (c-d) $Cu_2O$-10mgC after $CO_2RR$.

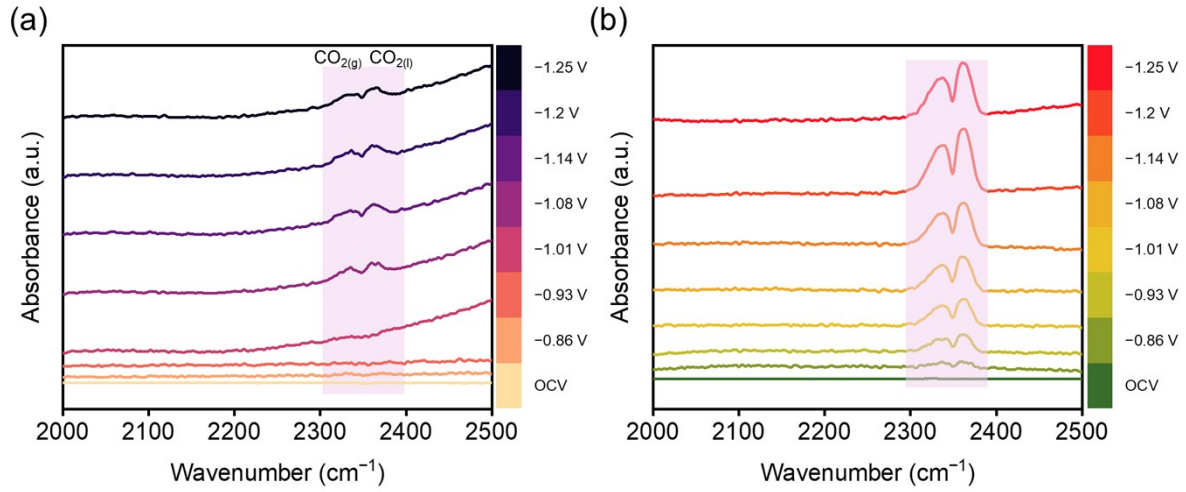


**Figure S19**. *In-situ* FT-iR spectra of the catalysts at OCV and over the potential range of −0.86 to −1.25 V: (a) $Cu_2O$; (b) $Cu_2O$−10mgC.

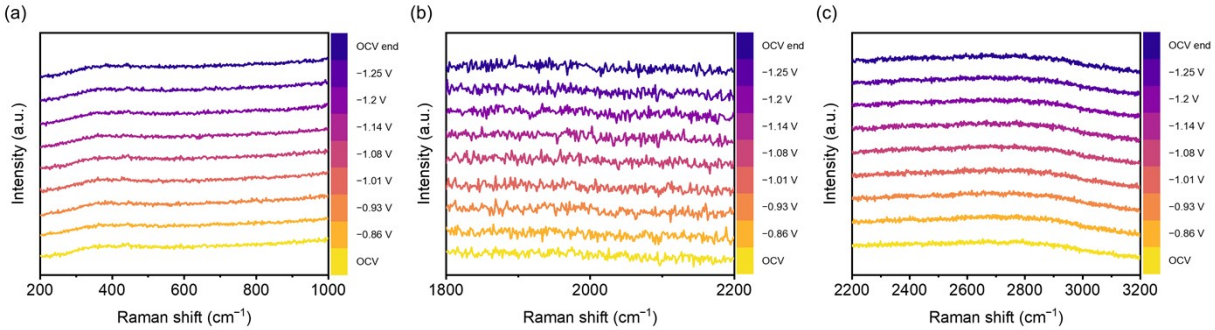


**Figure S20**. *In-situ* electrochemical Raman spectra of the AC catalyst in (a) 200 cm$^{-1}$ to 1000 cm$^{-1}$ , (b) 1800 cm$^{-1}$ to 2200 cm$^{-1}$ and (c) 2200 cm$^{-1}$ to 3200 cm$^{-1}$.

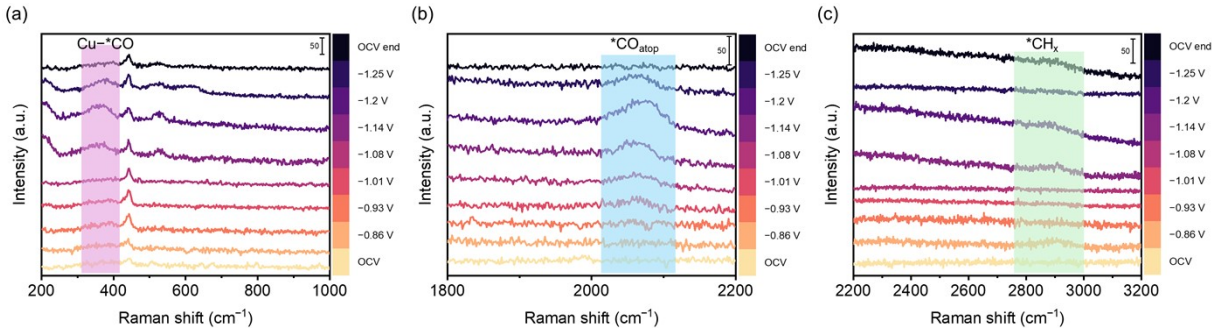


**Figure S21**. *In-situ* electrochemical Raman spectra of the $Cu_2O$ catalyst in (a) 200 $cm^{-1}$ to 1000 $cm^{-1}$ , (b) 1800 $cm^{-1}$ to 2200 $cm^{-1}$ and (c) 2200 $cm^{-1}$ to 3200 $cm^{-1}$.

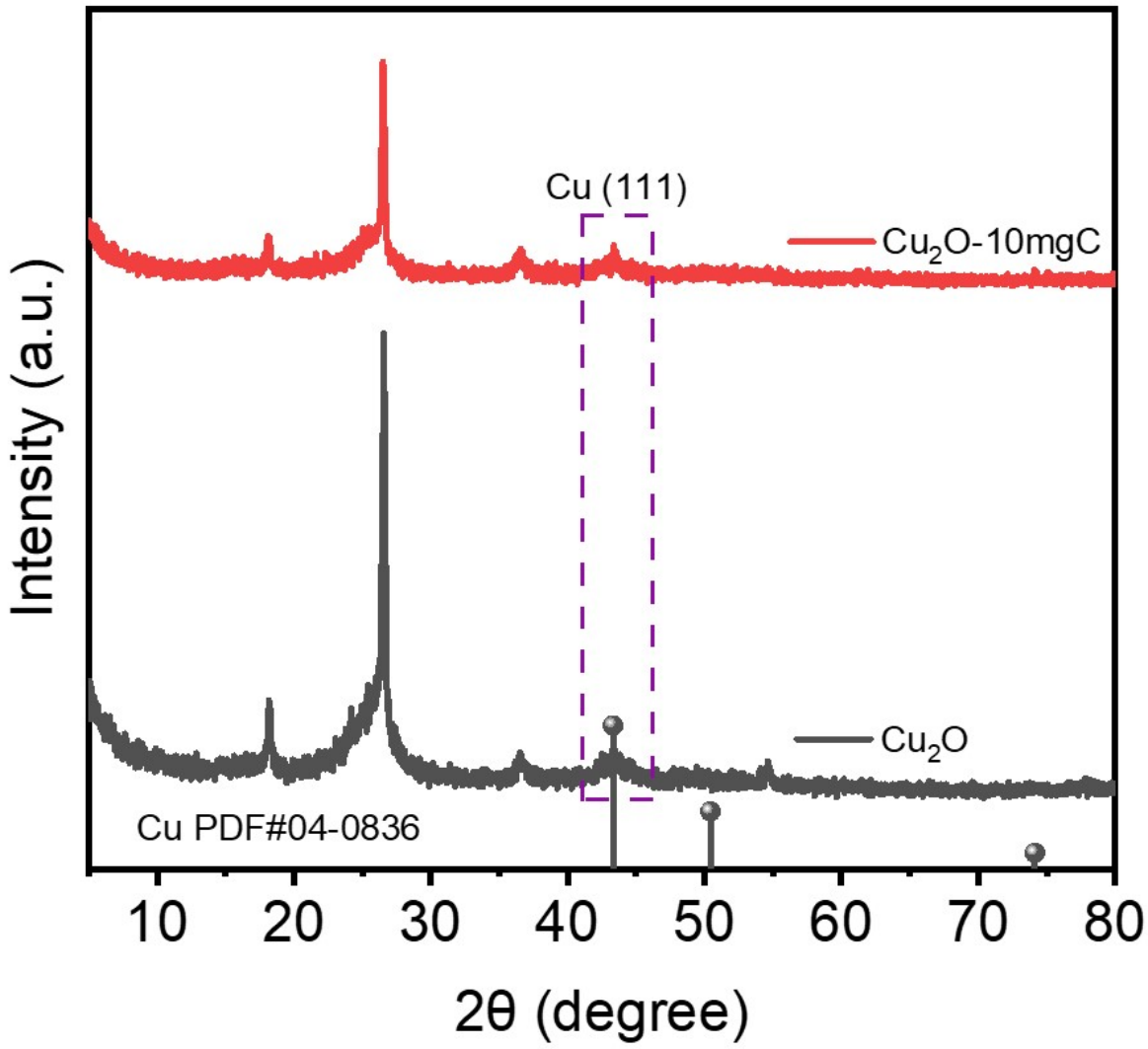


**Figure S22**. XRD patterns after $CO_2$RR of $Cu_2O$ and $Cu_2O$−10mgC.

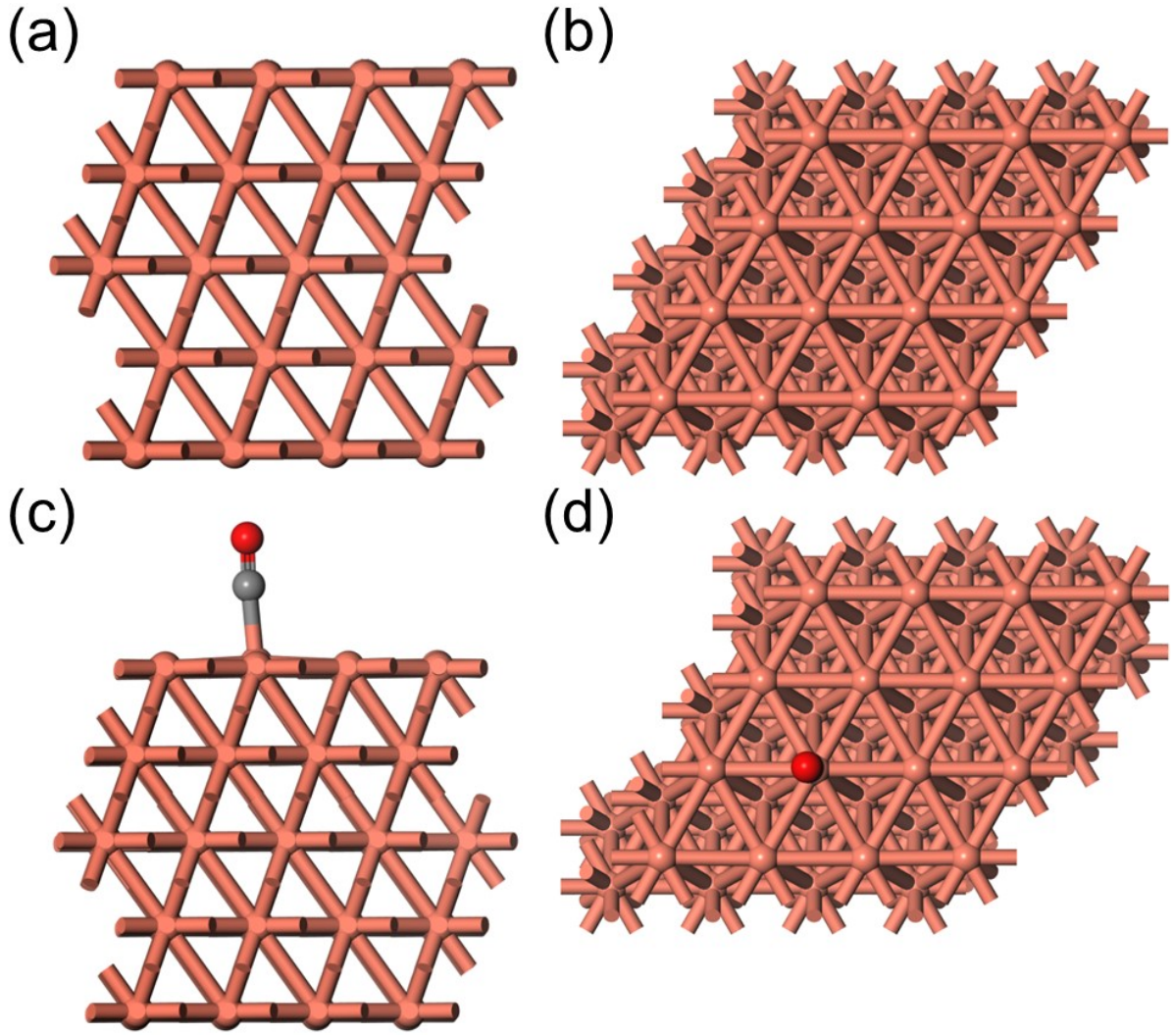


**Figure S23**. (a-b) Models of Cu (111), (c-d) Adsorption models of *CO on Cu (111).

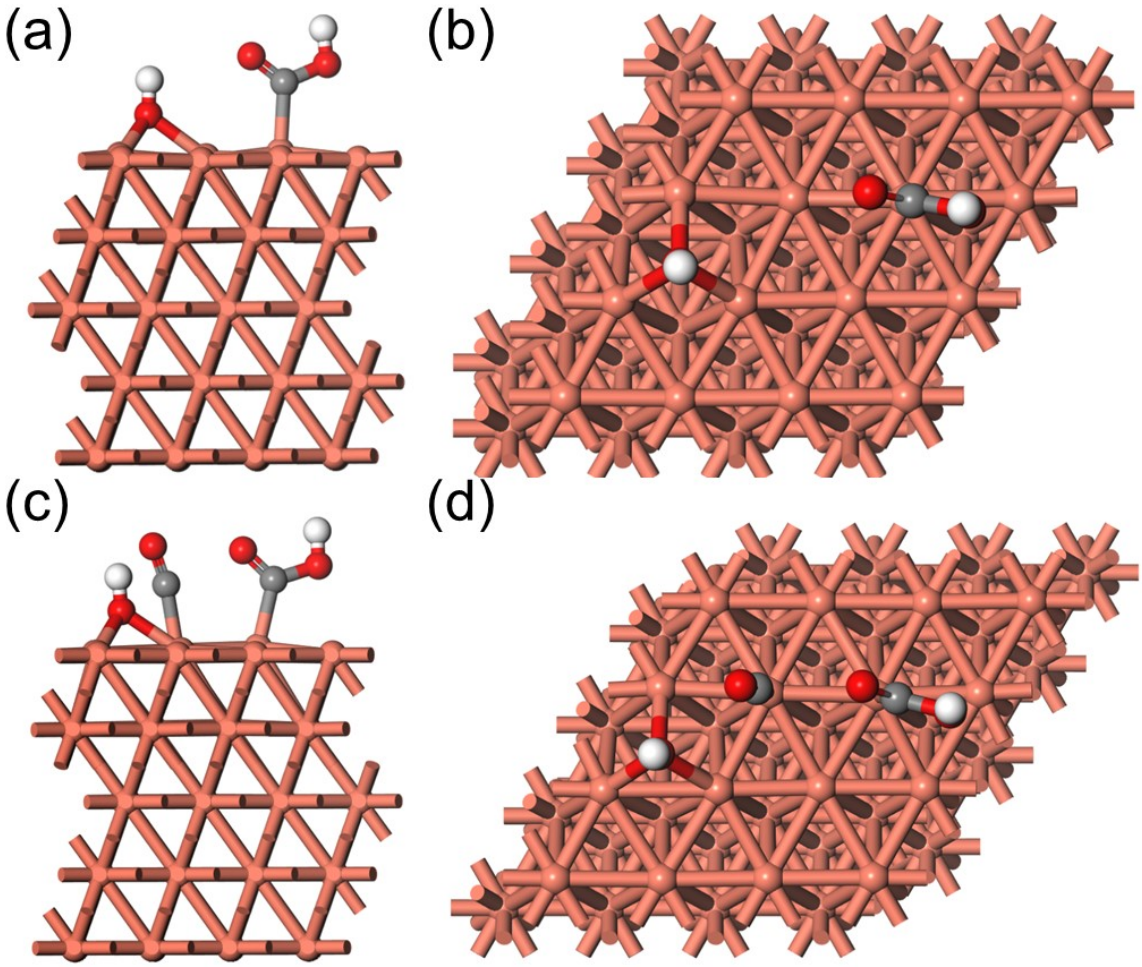


**Figure S24.** (a-b) Models of Cu (111)-center, (c-d) Adsorption models of *CO on Cu (111)-center.

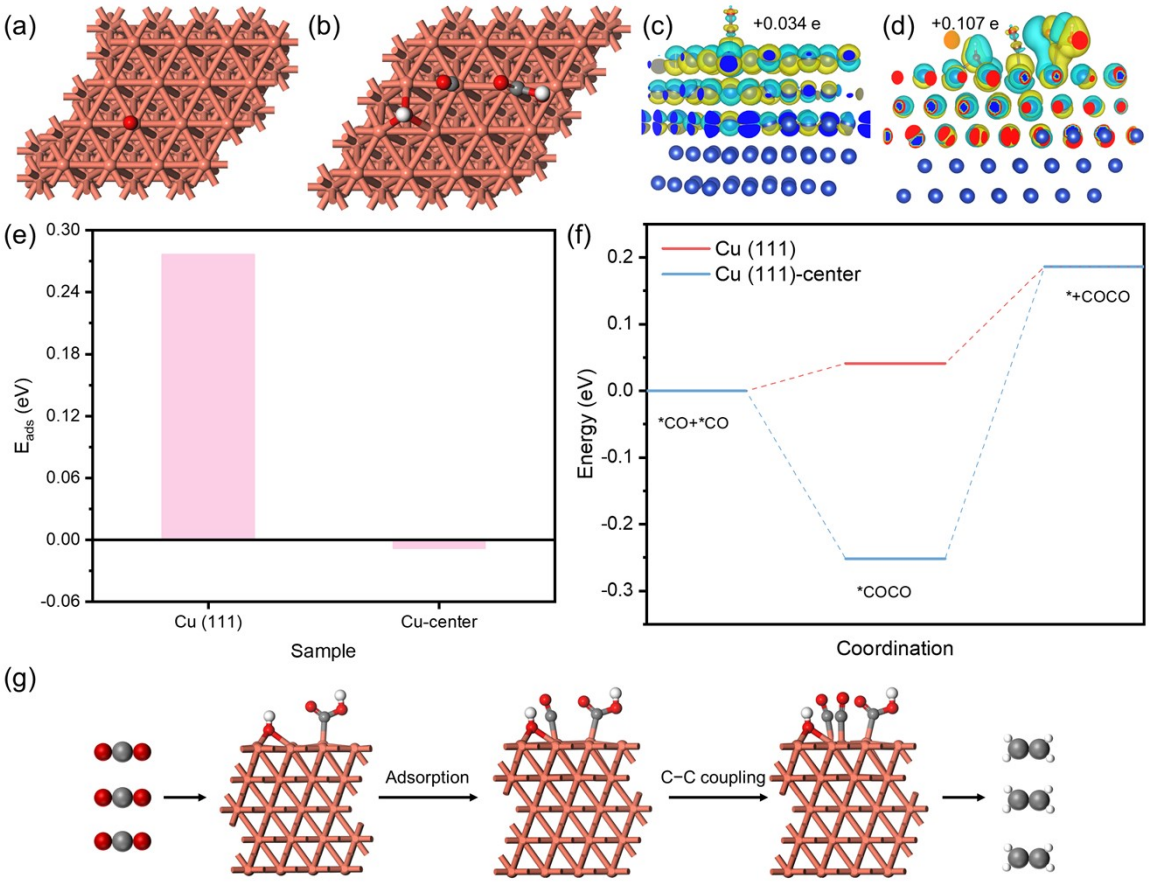


**Figure S25.** Adsorption modes of *CO on Cu (111) (a), Cu (111)-center (b). Deformation charge density and Bader charge of surface-adsorbed *CO in the Cu (111) (c), Cu (111)-center (d). (e) *CO adsorption energy on the Cu (111) and Cu (111)-center surface. (f) Free energy diagrams of *CO coupling to *COCO on Cu (111) and Cu (111)-center. (g) Proposed evolution of C−C coupling of $Cu_2O$−10mgC. The white, gray, red balls represent H, C, O atoms, respectively.

**Reference**

1. Kresse. G., Furthmuller. J., Efficiency of ab-initio total energy calculations for metals and semiconductors using a plane-wave basis set. Comp. Mater. Sci. **1996**, *6*, 15-50.
2. Kresse. G., Furthmuller. J., Efficient iterative schemes for ab initio total-energy calculations using a plane-wave basis set. Phys Rev B Condens Matter 1996, *54*, 11169-11186.
3. Blochl. P. E., Projector augmented-wave method. Phys Rev B Condens Matter **1994**, *50*, 17953-17979.
4. Perdew. J. P., Burke. K., Ernzerhof. M., Generalized Gradient Approximation Made Simple. Phys Rev Lett **1996**, *77*, 3865-3868.
5. Hammer. B., Hansen. L. B., Nørskov. J. K., Improved adsorption energetics within density-functional theory using revised Perdew-Burke-Ernzerhof functionals. Phys Rev B **1999**, *59*, 7413-7421.
6. Grimme. S., Antony. J., Ehrlich. S., Krieg. H., A consistent and accurate ab initio parametrization of density functional dispersion correction (DFT-D) for the 94 elements H-Pu. J Chem Phys **2010**, *132*, 154104.
7. Monkhorst. H. J., Pack. J. D., Special points for Brillouin-zone integrations. Phys Rev B **1976**, *13*, 5188-5192.